

# Iridium-PHOX-mediated alkene hydrogenation: Isomerization influences the stereochemical outcome

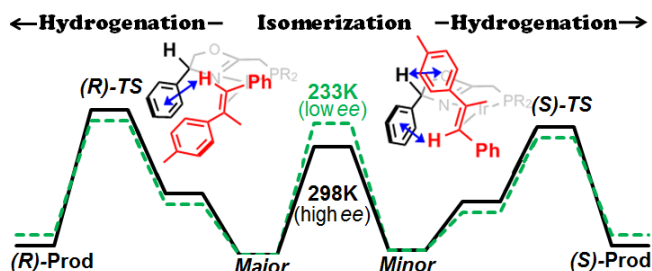
Kathrin H. Hopmann,<sup>\*,#,&</sup> Luca Frediani,<sup>#,&</sup> Annette Bayer<sup>&</sup>

<sup>#</sup>Centre for Theoretical and Computational Chemistry (CTCC) and <sup>&</sup>Department of Chemistry, University of Tromsø - The Arctic University of Norway, N-9037 Tromsø, Norway.

**Keywords:** Hydrogenation, phosphinoxazoline, enantioselectivity, empirical dispersion, iridium, DFT

Supporting Information Placeholder

**ABSTRACT** Recent experimental studies of iridium-phosphinoxazoline-mediated alkene hydrogenation indicated two dihydride intermediates as resting states, with the minor isomer assumed to give rise to the major product enantiomer [Gruber and Pfaltz, *Angew. Chem. Int. Ed.* **2014**, 53, 1896]. B3LYP-D2 calculations confirm the two dihydride intermediates as resting states, but show that these species do not give rise to the lowest-lying hydrogenation barriers. Instead, both species prefer to isomerize to different intermediates prior to hydrogenation. The computed enantiomeric excess (*ee*) at 298 K is in excellent agreement with experiment. The calculations further show an increased barrier for dihydride isomerization at lower temperature. Numerical simulations of the overall reaction kinetics indicate that this can explain the reduced enantioselectivity observed experimentally at 233 K. Analysis of the selectivity-determining interactions identifies strong CH/ $\pi$  interactions between the oxazoline substituents and the alkene. On basis of the insights obtained, a rational re-design of the catalyst is suggested, resulting in an improved *ee in silico*. Additional benchmark studies on different experimentally reported barriers and reaction energies for iridium complexes confirm the suitability of the employed computational protocol.



## Introduction

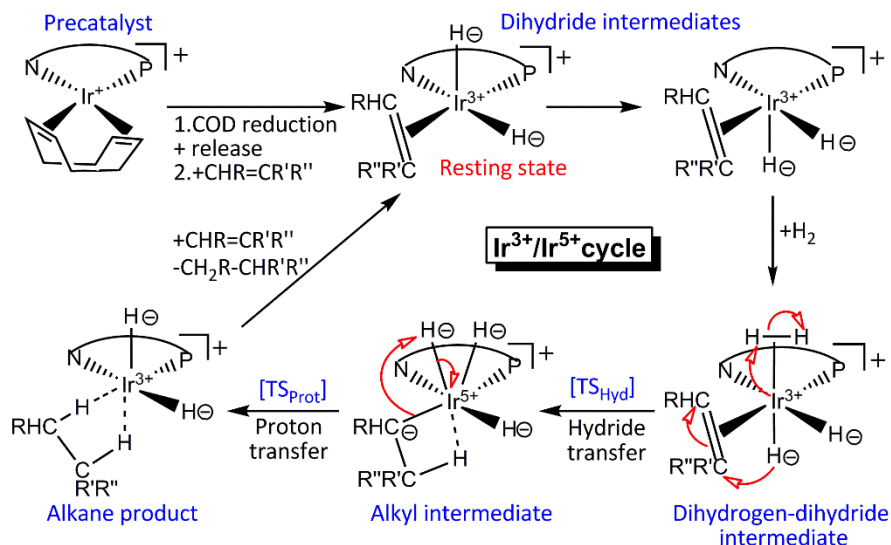
Chiral iridium-phosphinoxazoline (Ir-PHOX) complexes are versatile catalysts for the enantioselective hydrogenation of alkenes and imines.<sup>1,2,3,4</sup> These complexes can be viewed as chiral mimics of the *N,P* catalysts originally developed by Crabtree and coworkers.<sup>5</sup> Despite their successful applications in asymmetric hydrogenations, in particular of unfunctionalized substrates, high enantiomeric excesses are still restricted to a limited number of substrates (for a recent comprehensive review on *N,P*-Ir catalysts in alkene hydrogenation, see [6]). Further rational improvement of this type of catalysts is dependent on a detailed understanding of the reaction mechanisms and the selectivity-determining factors. Theoretical and experimental studies of Ir-PHOX-mediated alkene hydrogenation have provided important mechanistic insights,<sup>7,8,9,10,11</sup> but the selectivity-determining factors, which are substrate and ligand dependent, are little explored.<sup>8,11</sup>

The currently accepted inner-sphere mechanism for Ir-PHOX-mediated alkene hydrogenation was originally proposed by Brandt *et al.* on the basis of density functional theory (DFT) calculations on a truncated catalyst model.<sup>7</sup> Our theoretical studies on a full model of Ir-PHOX confirmed this mechanism and provided a rationale for the stereochemical outcome of alkene hydrogenation.<sup>7</sup> Additional studies by

Andersson and coworkers on a related thiazole-based complex,<sup>12</sup> and by Sparta *et al.* on an Ir-PHOX catalyst,<sup>11</sup> have further confirmed that alkene hydrogenation occurs through an Ir(III)/Ir(V) reaction cycle. In the first step, the substrate undergoes migratory insertion into an iridium-hydride bond, concomitantly with oxidative addition of a coordinated H<sub>2</sub> molecule (Scheme 1). This step is rate-limiting and determines the enantioselectivity of the reaction.<sup>7,11</sup> In the following step, a proton is transferred to the alkyl, resulting in generation of the alkane product and reduction of the metal.<sup>7,8</sup>

Our earlier quantum chemical calculations have shown that coordination of H<sub>2</sub> to the alkene-coordinated iridium complex is endergonic.<sup>7</sup> We therefore assumed that the resting state of the complex (in weakly coordinating solvent such as CH<sub>2</sub>Cl<sub>2</sub>) is a dihydride-Ir(III) intermediate, with an alkene molecule coordinated *trans* to phosphorous and a free apical coordination site (Scheme 1). In an elegant NMR study, Gruber and Pfaltz recently confirmed the existence of this dihydride reaction intermediate,<sup>10</sup> proposed as resting state (Scheme 1).<sup>8</sup> With catalyst **C1** and alkene **A1**, two isomers of the dihydride species were observed at 233 K, in a ratio of 11:1 (Fig. 1).<sup>10</sup> The two isomers coordinate the alkene from different faces, implying that the major isomer would form the (*R*)-alkane and the minor isomer would form the (*S*)-alkane. Interestingly, **C1**

## Scheme 1. Alkene Hydrogenation Mechanism of Ir-PHOX



<sup>a</sup>Based on the original proposal by Brandt *et al.*<sup>7</sup> and our DFT calculations.<sup>8</sup> Formal charges (corresponding to an ionic bonding model) are indicated to illustrate the electron flow.

mediated hydrogenation of **A1** gave the (*S*)-alkane with an enantiomeric excess (*ee*) of 72% at 233 K and 94% at 298 K.<sup>10</sup> It was therefore postulated that the major alkane enantiomer is formed from the minor dihydride isomer.<sup>10</sup>

The hydrogenation of alkene **A1** with catalyst **C1** was here evaluated through quantum chemical modeling employing B3LYP including the Grimme empirical dispersion correction D2.<sup>13</sup> Several recent studies have shown that B3LYP combined with empirical dispersion is able to provide excellent predictions of the enantioselectivity of iridium-catalyzed hydrogenation reactions.<sup>8,11,14</sup> The present study confirms the two experimentally observed dihydride intermediates as resting states, but shows that these prefer to isomerize to different intermediates prior to hydrogenation of the coordinated alkene. The calculations further provide a possible explanation for the different enantiomeric excesses obtained at respectively 233 K and 298 K in experiments. Identification of the selectivity-determining interactions allows us to predict a catalyst modification leading to an improved enantiomeric excess *in silico*.

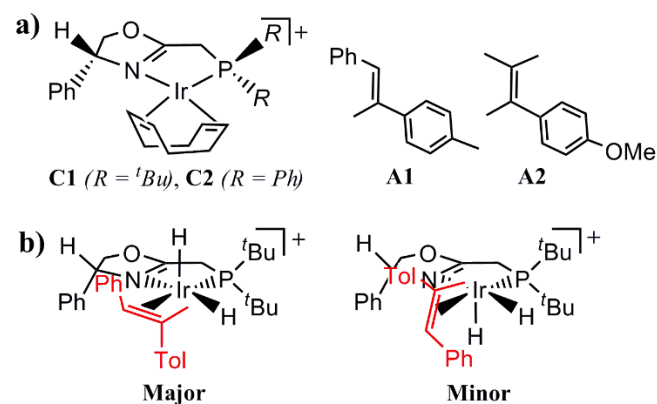


**Figure 1.** a) Catalysts and alkenes evaluated here, b) Dihydride species formed from **C1** and **A1** in experiments (11:1 at 233 K, adapted from [10]).

## Computational Details

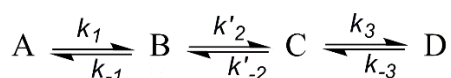
Full catalysts (**C1**, **C2**) and full substrates (**A1**, **A2**) models were employed (Fig. 1). Calculations were performed using the hybrid density functional B3LYP<sup>15</sup> as implemented in Gaussian 09 (Rev. B.01).<sup>16</sup> Also included in all calculations were the implicit solvent model IEFPCM<sup>17</sup> (CH<sub>2</sub>Cl<sub>2</sub>, including only the electrostatic terms) and the Grimme empirical dispersion correction D2,<sup>13</sup> which contains parameters up to R<sub>n</sub> in the employed Gaussian revision. Geometry optimizations were performed with the basis set 6-311G(d,p) on all atoms, except iridium, for which the basis set and effective core potential LANL2DZ<sup>18</sup> were employed, augmented with an *f* polarization function (exponent 0.65). Thermochemical quantities were obtained from frequency calculations at the same level of theory as the geometry optimizations, with temperature corrections of 233 K or 298 K. The nature of optimized transition states was confirmed through frequency calculations (all exhibiting a single imaginary frequency) and, for selected species, through additional IRC calculations. Single-point calculations were performed on all optimized geometries with the larger 6-311+G(2d,2p) basis set on all non-metallic atoms and LANL2TZ(f)<sup>18,19</sup> on iridium to obtain more accurate electronic energies. Final energies are Gibbs free energies. Note that these correspond to a standard state of 1 atm (0.041 M), unless clearly stated otherwise.<sup>20</sup>

For calculating the cost of dissociating **A1** from **C1**, a counterpoise (CP) correction as defined in [21] was computed, which amounted to 2.0 kcal/mol at the bigger basis set. CP corrections were also computed for species formed through coordination of H<sub>2</sub> to iridium (amounting to 0.4 kcal/mol).

Key results obtained here were reevaluated with different functionals (B3LYP, MO6, MO62X<sup>22</sup>) in combination with different type of Grimme dispersion corrections (D2<sup>13</sup> or D3,<sup>23</sup> see SI for details).

The time evolution of the concentrations was modeled with a simplified reaction path involving four species: the two

dihydride intermediates B (major) and C (minor) and the two hydrogenated products A ((*R*)-alkane) and D ((*S*)-alkane):



The following assumptions were made: (i) no back-reaction from A to B or from D to C ( $k_{-1} = k_{-3} = 0$ ), (ii) hydrogen concentration constant and unitary, (iii) initial B/C ratio given by their computed free energy difference, (iv) rate constants derived from transition state theory<sup>21</sup> employing the computed free energies. The set of four coupled linear differential equations yielding the concentration of each species in time can be easily integrated to provide an estimate of the enantiomeric excess (see SI for details).

## Results and Discussions

### Dihydride species and isomerization

NMR studies of H<sub>2</sub> addition to a square-planar Ir-PHOX complex in THF have identified two dihydride species, one with a hydride above the basal plane, and one with a hydride below.<sup>9</sup> Coordination of a prochiral alkene such as **A1** to the equivalent **C1**-based dihydrides can give rise to 8 possible dihydride isomers (Fig. 2). The B3LYP-D2 optimized geometries reveal that dispersion interactions between the substrate substituents (H,Ph/Tol) and the substituents on the chiral carbon of the oxazoline ring (optimized coordinates are given as supporting information). For four of the stereoisomers, this results in placement of the alkene double bond in the basal plane (**DiH-1** to **DiH-4**), whereas for the other four, the double bond is tilted towards aligning with the axial hydride (**DiH-5** to **DiH-8**, Fig. 2). The computed free energies show that the two lowest-lying dihydride species are **DiH-1** and **DiH-6** (Figure 2). Gratifyingly, these two species correspond to the two isomers that in experiments were identified as the major and the minor isomer (Fig. 1). The computed relative energy difference of 0.7 kcal/mol (233 K) corresponds to a Boltzmann distribution of 5:1 for

these two isomers, in good agreement with the experimentally observed distribution of 11:1 at 233 K.<sup>10</sup>

Gruber and Pfaltz show evidence for fast isomerization between the major and the minor dihydride species.<sup>10</sup> Given that the alkene is bound from opposite faces in these two species, isomerization requires dissociation and re-binding of the alkene. The here proposed reaction pathway for isomerization between the dihydride species and corresponding computed energies are illustrated in Figure 3. Flipping of the hydrides in **DiH-1** to form **DiH-2** has a barrier of 6.4 kcal/mol (TS<sub>flip</sub>). Dissociation of **A1** from the complex costs 16.8 kcal/mol at 298 K (20.4 kcal/mol at 233 K, Fig. 3), which here is assumed to represent the overall barrier for isomerization.<sup>24,25</sup> The alkene can then rebind from the opposite face, forming dihydride **DiH-6**. A solvent molecule might temporarily coordinate to the iridium centre, but this would not reduce the initial cost of dissociating **A1**. Concerted alkene dissociation and solvent binding through an interchange mechanism is, for sterical reasons, not possible. An alternative pathway to Figure 3, proceeding through **DiH-5**, was found 2 kcal/mol higher in energy.

### Dihydrogen-dihydride species and isomerization

Hydrogenation of the coordinated alkene requires binding of an H<sub>2</sub> molecule to the dihydride complex (Scheme 1). Coordination of H<sub>2</sub> in the vacant coordination site of the dihydride isomers (Fig. 2) gives rise to eight dihydrogen-dihydride species (Table 1). Of these, the preferred dihydrogen-dihydride isomers are **H<sub>2</sub>-DiH-1** and **H<sub>2</sub>-DiH-5** (Table 1), respectively formed from **DiH-1** and **DiH-5** (H<sub>2</sub> binding below the basal plane in both cases, Fig. 2). For all substrate-coordinated dihydrogen-dihydrides, H<sub>2</sub> binding below the basal plane appears preferred. A similar trend was observed earlier.<sup>8</sup>

The dihydrogen-dihydride isomers can also isomerize. If dissociation of the alkene is required, calculations show that it is more favorable to isomerize without H<sub>2</sub> coordinated, i.e. as in Figure 3. However, for isomerization between species only differing in the position of the H<sub>2</sub> molecule (above or below

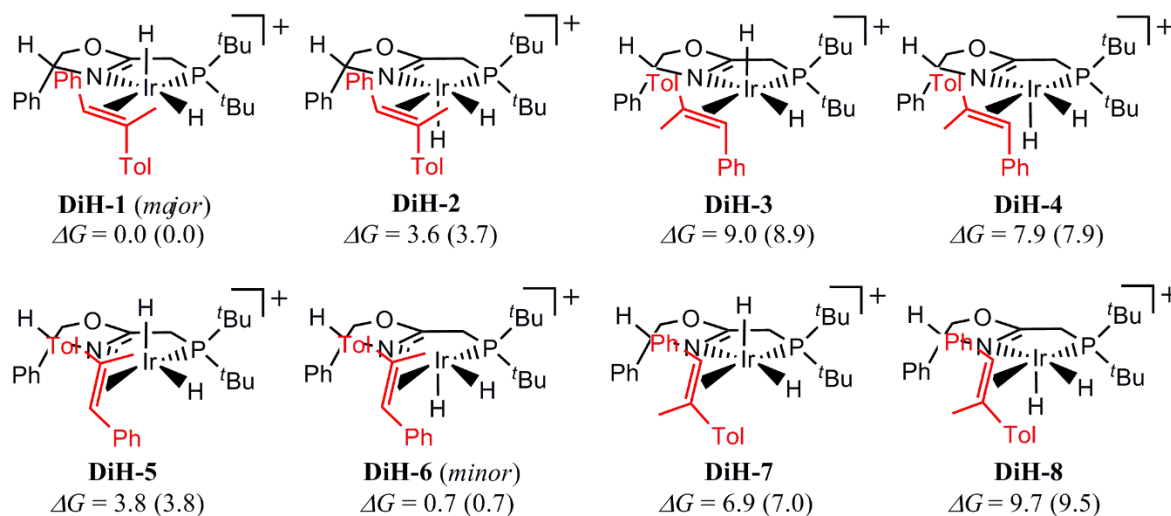


**Figure 2.** Eight dihydride isomers formed from **C1** and **A1**. Schematic representation of optimized geometries and relative Gibbs free energies in kcal/mol (298 K, in parentheses 233 K). **DiH-1** to **DiH-4** have a pro-(*R*) and **DiH-5** to **DiH-8** a pro-(*S*) configuration.

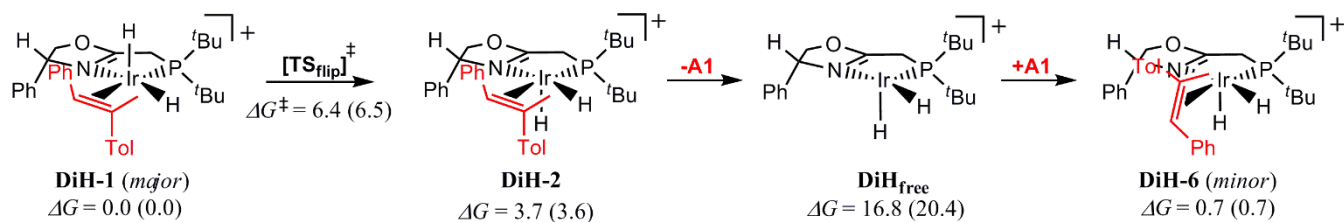


**Figure 3.** Isomerization of the major (**DiH-1**) to the minor (**DiH-6**) dihydride species requires alkene dissociation. Schematic representation of optimized geometries and relative Gibbs free energies in kcal/mol (298 K, in parentheses 233 K).

**Table 1. Computed relative energies<sup>a</sup> (kcal/mol) for dihydrogen-dihydride isomers formed from C1 and A1.**

Isomer	$\Delta G_{298\text{K}}$ ( $\Delta G_{233\text{K}}$ )	Stereo <sup>b</sup>
<b>H<sub>2</sub>-DiH-1</b> (from major)	<b>7.6 (6.0)</b>	pro-( <i>R</i> )
<b>H<sub>2</sub>-DiH-2</b>	9.5 (7.8)	pro-( <i>R</i> )
<b>H<sub>2</sub>-DiH-3</b>	13.1 (11.1)	pro-( <i>R</i> )
<b>H<sub>2</sub>-DiH-4</b>	14.0 (12.4)	pro-( <i>R</i> )
<b>H<sub>2</sub>-DiH-5</b>	<b>8.3 (6.6)</b>	pro-( <i>S</i> )
<b>H<sub>2</sub>-DiH-6</b> (from minor)	10.1 (8.5)	pro-( <i>S</i> )
<b>H<sub>2</sub>-DiH-7</b>	11.7 (10.1)	pro-( <i>S</i> )
<b>H<sub>2</sub>-DiH-8</b>	18.3 (16.8)	pro-( <i>S</i> )

<sup>a</sup>) Relative to **DiH-1** and free H<sub>2</sub>. <sup>b</sup>) Alkene coordination mode.

the basal plane), facile one-step isomerization can be achieved (Figure 4). The isomerization does not proceed through a tetrahydride-Ir(V)-intermediate (as might have been expected<sup>26</sup>) but occurs in a single step, through concerted dihydrogen splitting, proton shuttling, and dihydrogen reformation, resulting in direct interconversion of two dihydrogen-dihydride-Ir(III) species. This is somewhat reminiscent of a  $\sigma$ -complex-assisted metathesis ( $\sigma$ -CAM) mechanism,<sup>27</sup> however, in the transition state here, two  $\sigma$ -CAM rearrangements occur concertedly, instead of through a distinct intermediate.

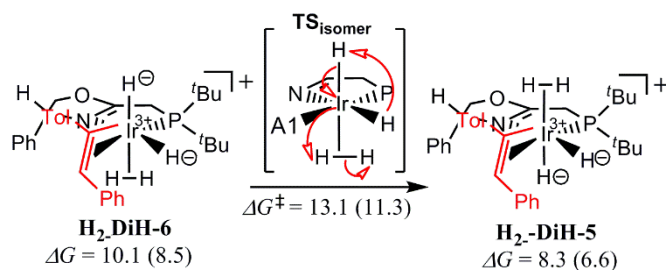


**Figure 4.** Single-step isomerization between two dihydrogen-dihydride-Ir(III) complexes (energies in kcal/mol, 298 K (233K)). Formal charges are indicated to illustrate the electron flow.

The relative energies of the dihydrogen-dihydride species indicate that once H<sub>2</sub> has coordinated to **DiH-6** to form **H<sub>2</sub>-DiH-6**, this species would prefer to isomerize to **H<sub>2</sub>-DiH-5**, which is 1.8 kcal/mol lower in energy (Table 2). The barrier for the single-step isomerization is 13.1 kcal/mol (298 K, Fig. 4). Note that the alkene coordination mode remains identical

for this type of isomerizations, e.g. both **H<sub>2</sub>-DiH-6** and **H<sub>2</sub>-DiH-5** are pro-(*S*). However, the barrier heights for subsequent steps might be different, affecting the enantioselectivity, as shown in the following section.

### Enantioselectivity

Following H<sub>2</sub> coordination, the next reaction step involves hydride transfer to the coordinated substrate (Scheme 1). This step is rate-limiting and determines the enantioselectivity of Ir-PHOX-mediated alkene hydrogenation.<sup>7,11</sup> Here, the hydride transfer transition states were computed for all dihydrogen-dihydride isomers formed from **C1** and **A1** (TS<sub>Hyd-1</sub> to TS<sub>Hyd-8</sub>, Table 2). Hydride transfer can occur from above or below the basal plane (transfer in the plane results in large overall barriers).<sup>7,11</sup> For alkenes coordinated in the basal plane (**DiH-1** to **DiH-4**, Fig. 2), this requires rotation of the alkene such that the double bond is aligned with the axial Ir-hydride bond. Rotation is expected to occur in the direction with least steric hindrance, i.e. clock-wise. The optimized transition state structures are shown schematically in Figure S1, SI. Note that also alternative hydrogenation mechanisms besides the one in Scheme 1 were evaluated, but these exhibited higher barriers (Scheme S1, SI). It was also evaluated if formation of the (*Z*)-form of **A1** might be relevant during hydrogenation, but this is considered very unlikely (Scheme S2, SI).

The computed results reveal that the hydride transfer barrier of **H<sub>2</sub>-DiH-6** (formed from the minor species) is 0.8 kcal/mol lower than that of **H<sub>2</sub>-DiH-1** (formed from the major species, see TS<sub>Hyd-6</sub> versus TS<sub>Hyd-1</sub>, Table 2). This would be in agreement with the prediction by Gruber and Pfaltz that the minor species gives rise to the observed (*S*)-alkane formation.<sup>10</sup> However, interestingly, two different isomers, **H<sub>2</sub>-DiH-2** and **H<sub>2</sub>-DiH-5**, provide hydride transfer transition states with significantly lower barriers (TS<sub>Hyd-2</sub> and TS<sub>Hyd-5</sub>, Table 2). We therefore predict that the latter two intermediates, and not the dihydrogen-complexes formed from the resting states (**H<sub>2</sub>-DiH-1** and **H<sub>2</sub>-DiH-6**) determine the stereochemical outcome.

Figure 5 illustrates the hydrogenation and isomerization barriers of the relevant species. For both **H<sub>2</sub>-DiH-1** and **H<sub>2</sub>-DiH-6** it is preferable to isomerize to respectively **H<sub>2</sub>-DiH-2** and **H<sub>2</sub>-DiH-5** prior to hydrogenation. The barriers for isomerization between the dihydrogen-dihydride species (TS<sub>isomer</sub>, Figure 4) are >6 kcal/mol lower than the hydrogenation barriers, implying that this type of isomerization occurs at a much faster rate (isomerization can also occur prior to H<sub>2</sub> binding, with an even lower barrier, see TS<sub>flip</sub>, Figure 3).

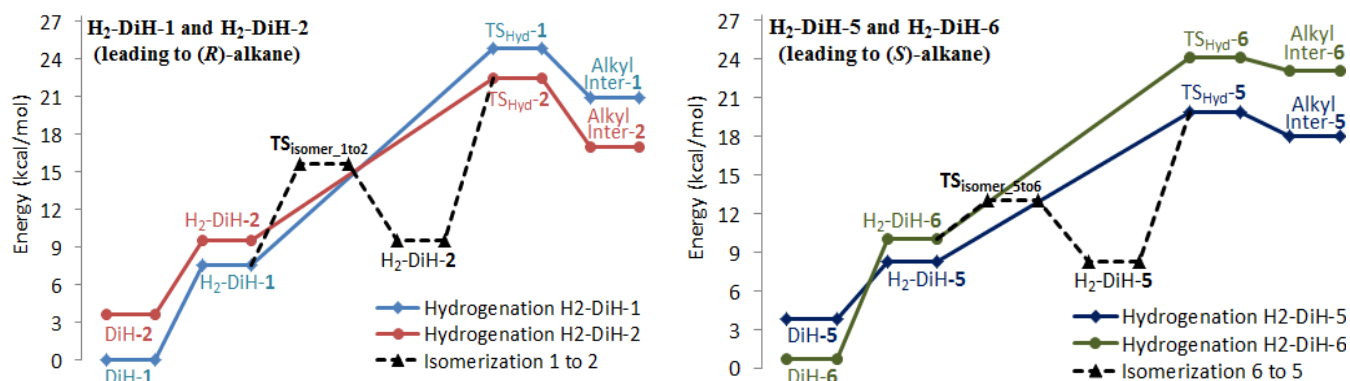


**Figure 5.** Computed Gibbs free energies for the hydride transfer step ( $TS_{Hyd}$ ) of the lowest-lying pro-(*R*) dihydrogen-dihydrides **H<sub>2</sub>-DiH-1** and **H<sub>2</sub>-DiH-2** (left) and pro-(*S*) dihydrogen-dihydrides **H<sub>2</sub>-DiH-5** and **H<sub>2</sub>-DiH-6** (right). Also shown are the barriers for isomerization between dihydrogen-dihydride intermediates ( $TS_{isomer}$ , Fig. 4). Energies are relative to **DiH-1** and free H<sub>2</sub>.

The experimentally determined *ee* of **C1**-mediated hydrogenation of **A1** is 94% (*S*) at 298K.<sup>10</sup> Assuming that hydrogenation occurs through intermediates **H<sub>2</sub>-DiH-2** and **H<sub>2</sub>-DiH-5** (Fig. 5), the computed  $\Delta\Delta G^{\ddagger}_{R,S}$  at 298K is 2.6 kcal/mol (Table 2). This corresponds to an *ee* of 98% (*S*), in very good agreement with experiment.<sup>10</sup> If hydrogenation instead occurred through **H<sub>2</sub>-DiH-1** and **H<sub>2</sub>-DiH-6** (formed directly from the minor and the major species), the computed *ee* would be much lower, 58% (*S*) at 298 K ( $\Delta\Delta G^{\ddagger}_{R,S} = 0.8$  kcal/mol, Table 2). The computed energies for the full hydrogenation reaction pathways, starting from the resting states and proceeding through **H<sub>2</sub>-DiH-2** and **H<sub>2</sub>-DiH-5**, are depicted in Figure 6. Note that all energies are given relative to the major species (**DiH-1** + free H<sub>2</sub>), i.e. the alkene-coordinated complex. The free energy change for conversion of **A1** to alkane is thus not directly evident from the graph; this is -15.0 kcal/mol (298 K) in our calculations.

Interestingly, the experimentally determined *ee* of **C1**-mediated hydrogenation of **A1** at 233 K is 72% (*S*).<sup>10</sup> The computed results show that also at 233 K, hydrogenation preferably proceeds through intermediates **H<sub>2</sub>-DiH-2** and **H<sub>2</sub>-DiH-5**, with a  $\Delta\Delta G^{\ddagger}_{R,S}$  of 2.6 kcal/mol (Table 2). At 233 K,

this corresponds to an *ee* of 99% (*S*) and does not match the experimental *ee*.<sup>10</sup> It is proposed here that the enantioselectivity at 233 K is influenced by the barrier for dihydride isomerization (Figure 3). Only if isomerization between intermediates is fast relative to hydrogenation, is it possible to assume that the enantioselectivity is solely determined by the relative hydrogenation barriers (Curtin-Hammett principle). This scenario is fulfilled at 298 K, but not at 233 K (Figure 6). At 233 K, the computed isomerization barrier is larger than the hydrogenation barrier for forming the (*S*)-alkane, implying that it is necessary to simulate the reaction kinetics numerically in order to predict the stereoselective outcome. Such a simulation was carried out here with a simplified reaction path including only the rate-limiting steps for hydrogenation and isomerization, with the rate constants obtained from the computed free energies (for details see SI).

The numerically simulated concentrations of the major (**DiH-1**) and minor (**DiH-6**) dihydride species and the hydrogenated products ((*S*)- and (*R*)-alkane) are shown in Figure 7. The numerical model predicts that at 298 K, the major and minor species stay in equilibrium during the hydrogenation reaction (Figure 7, right). The predicted *ee* becomes 97% (*S*), further confirming the validity of the Curtin-Hammett principle in this case. At 233 K, the simulation shows non-equilibrium conditions for the major and minor species (Figure 7, left). The numerical modelling predicts a resulting *ee* of 23% (*S*), implying that the selectivity, which would be 99% on the basis of the  $\Delta\Delta G^{\ddagger}_{R,S}$  value only, is significantly reduced due to the increased isomerization barrier. In order to obtain the experimental *ee* of 72% (*S*) at 233 K from the numerical model, the barrier for isomerization (equaling the cost of alkene dissociation) should be reduced by only 0.7 kcal/mol (Figure S4, SI). Note that dissociation energies generally are challenging to compute and might have an error of several kcal/mol, dependent on the computational protocol employed (*vide infra*).<sup>25,28,29</sup> In addition, note that the energies reported here are standard state free energies ( $\Delta G^\circ$ ), i.e. in experiments, the relative energies will be further affected by the reaction conditions (such as solute concentrations and H<sub>2</sub> pressure).

**Table 2. Hydride transfer barriers<sup>a</sup> (kcal/mol) for dihydrogen-dihydride isomers formed from **C1** and **A1**.<sup>b</sup>**

	$\Delta G^{\ddagger}_{298K}$ ( $\Delta G^{\ddagger}_{233K}$ )	Stereo <sup>c</sup>
<b>TS<sub>Hyd</sub>-1</b> (from major)	<b>24.9 (22.8)</b>	pro-( <i>R</i> )
<b>TS<sub>Hyd</sub>-2</b>	<b>22.5 (20.8)</b>	pro-( <i>R</i> )
<b>TS<sub>Hyd</sub>-3</b>	28.6 (26.5)	pro-( <i>R</i> )
<b>TS<sub>Hyd</sub>-4</b>	28.4 (26.7)	pro-( <i>R</i> )
<b>TS<sub>Hyd</sub>-5</b>	<b>19.9 (18.2)</b>	pro-( <i>S</i> )
<b>TS<sub>Hyd</sub>-6</b> (from minor)	<b>24.1 (22.4)</b>	pro-( <i>S</i> )
<b>TS<sub>Hyd</sub>-7</b>	26.4 (24.6)	pro-( <i>S</i> )
<b>TS<sub>Hyd</sub>-8</b>	29.9 (27.7)	pro-( <i>S</i> )

<sup>a</sup>)Relative to **DiH-1** and free H<sub>2</sub>.<sup>b</sup>) For schematic TS geometries see Fig. S1, SI. <sup>c</sup>)Alkene coordination mode.

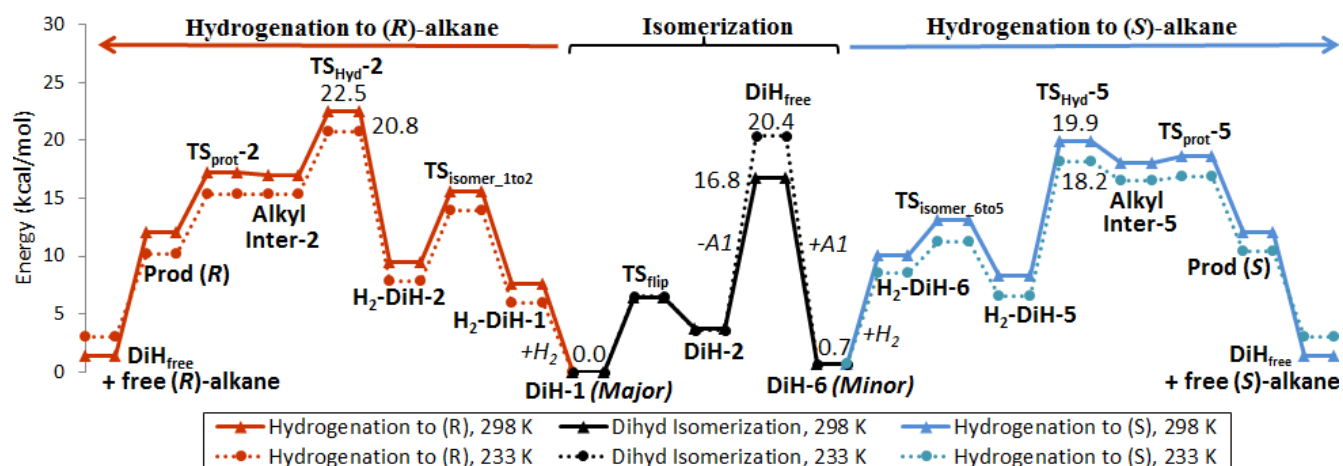


**Figure 6.** Computed relative Gibbs free energies for isomerization and **C1**-mediated hydrogenation of **A1** at 233 K (dashed line) and 298 K (solid line). Middle part illustrates the isomerization between the major and minor dihydride species (see Fig. 3 for mechanism), left the lowest hydrogenation pathway for formation of the (*R*)-alkane and right the lowest hydrogenation pathway for formation of the (*S*)-alkane.

#### Functional dependence of results and benchmark studies

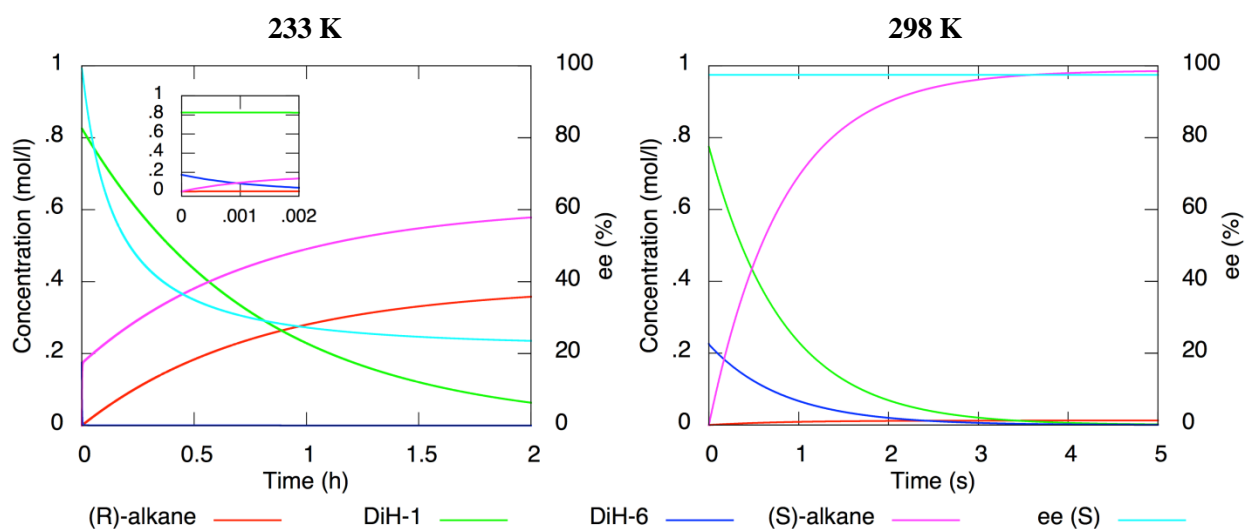
To evaluate the robustness of the presented results (obtained at the B3LYP-D2 level), several key steps were evaluated with different functionals and different types of Grimme dispersion corrections (D2<sup>13</sup> or D3<sup>23</sup>). The functional combinations are: B3LYP, B3LYP-D2, B3LYP-D3, M06, M06-D3, and M062X.

The ratio between the dihydride species **DiH-1** and **DiH-6** (11:1 at 233K, Fig.1)<sup>10</sup> is reproduced to within an error of 0.4 kcal/mol by B3LYP with D2 or D3 and by M06 (Table S1). However, M062X and M06-D3 incorrectly predict **DiH-6** to be the major species.

Optimization of the two lowest lying hydride transfer transition states, TS<sub>Hyd-5</sub> (pro-*S*) and TS<sub>Hyd-2</sub> (pro-*R*), Table 2) show that all tested functionals predict TS<sub>Hyd-5</sub> to be the lowest, with a remarkably similar predicted *ee* at 298 K of

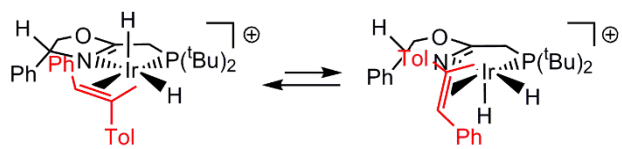
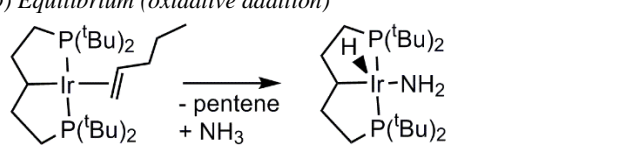
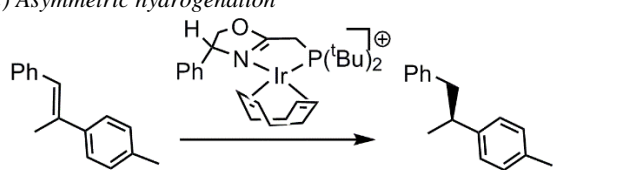
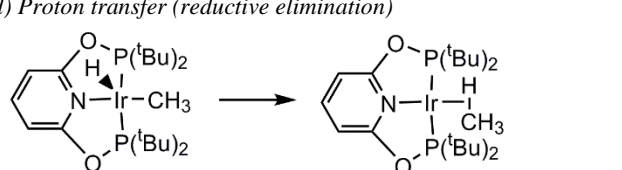
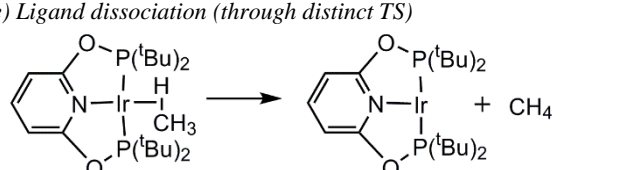
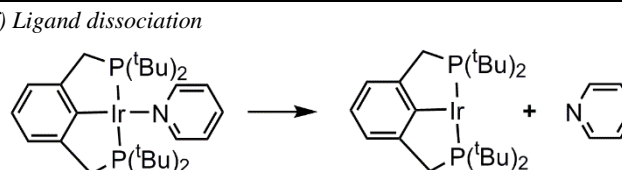
97.5 to 99.5 % (*S*) (Table S2). For this catalytic system, prediction of the major product thus does not depend on the choice of computational protocol.

The cost of dissociating **A1** from **C1** is found to be very functional dependent, as observed in similar studies on ligand binding energies.<sup>25,28,29</sup> Predicted values range from 7 to 23 kcal/mol for the 5 functionals tested (Table S3). The three lowest predictions originate from M06, M062X, and B3LYP-D3, which in other studies have been shown to underestimate dissociation energies, in some cases severely.<sup>25,29</sup> B3LYP-D2, however, performed well (and better than the other functionals evaluated here) in tests on 10 dissociation enthalpies in solution.<sup>25</sup> Additional benchmark studies performed here (*vide infra*) indicate that B3LYP-D2 provides reasonable errors for calculations of this type. The **A1** dissociation free energy



**Figure 7.** Numerical simulation of the reaction kinetics of **C1**-mediated hydrogenation of **A1** on basis of the computed Gibbs free energies. Graphical representation of the time evolution of the concentrations of the major (**DiH-1**) and minor (**DiH-6**) dihydride species, the hydrogenation products ((*R*)- and (*S*)-alkane), and the enantiomeric excess (*ee*) at 233 K (left) and 298 K (right).

**Table 3.** Benchmark of employed computational protocol (B3LYP-D2 with IEFPCM) against experimental results for different iridium based systems (all values in kcal/mol, unless otherwise stated).<sup>a</sup> B3LYP-D3 results are given for comparison.

Reaction type	Experimental quantity	Computed value	Error
(a) Equilibrium		<b>B3LYP-D2:</b> Ratio <sup>233K</sup> = 5:1 $\Delta G^{\circ,233K} = 0.8$	-0.3
	Ratio <sup>233K</sup> = 11:1 ( $\approx \Delta G^{\circ,233K} = \mathbf{1.1}$ ) in $CH_2Cl_2^b$	<b>B3LYP-D3:</b> Ratio <sup>233K</sup> = 9:1 $\Delta G^{\circ,233K} = 1.0$	-0.1
(b) Equilibrium (oxidative addition)		<b>B3LYP-D2:</b> $\Delta G^{\circ,298K} = -0.8$	+0.5
	$K_{eq} = 9$ at RT ( $\approx \Delta G^{\circ,298K} = \mathbf{-1.3}$ ) in diethyl ether <sup>c</sup>	<b>B3LYP-D3:</b> $\Delta G^{\circ,298K} = -3.6$	-2.3
(c) Asymmetric hydrogenation		<b>B3LYP-D2:</b> $ee^{298K} = 97.5\%$ (S) $\Delta \Delta G_{R-S}^{\neq,298K} = 2.6$	+0.5
	$ee^{298K} = 94\%$ (S) ( $\approx \Delta \Delta G_{R-S}^{\neq,298K} = \mathbf{2.1}$ ) in $CH_2Cl_2^b$	<b>B3LYP-D3:</b> $ee^{298K} = 98.2\%$ (S) $\Delta \Delta G_{R-S}^{\neq,298K} = 2.8$	+0.7
(d) Proton transfer (reductive elimination)		<b>B3LYP-D2:</b> $\Delta G^{\neq,168K} = 11.8$	+2.5
	$\Delta G^{\neq,168K} = \mathbf{9.3}$ in $CHCl_2F^d$	<b>B3LYP-D3:</b> $\Delta G^{\neq,168K} = 10.9$	+1.6
(e) Ligand dissociation (through distinct TS)		<b>B3LYP-D2:</b> $\Delta G^{\neq,303K} = 22.7$	+0.3
	$\Delta G^{\neq,303K} = \mathbf{22.4}$ in $CHCl_2F^e$		
(f) Ligand dissociation		<b>B3LYP-D2:</b> $\Delta G^{\circ,298K,1M} = 19.0$	-2.3
	$\Delta H^{\neq} = 24.9$ , $\Delta S^{\neq} = 12.1$ e.u. ( $\approx \Delta G^{\neq,298K} = \mathbf{21.3}$ ) in <i>p</i> -xylene <sup>f</sup>	<b>B3LYP-D3:</b> $\Delta G^{\circ,298K,1M} = 15.1$	-6.2

<sup>a</sup>See SI for further details, <sup>b</sup>From Ref. [10], <sup>c</sup>From Ref. [32], <sup>d</sup>From Ref. [30], reaction occurred in  $CHCl_2F$  or  $CHCl_3$ , computed in  $CHCl_3$  <sup>e</sup>From Ref. [30], reaction occurred in  $CHCl_2F$ , computed in  $CHCl_3$ , <sup>f</sup>From Ref. [31]. Assumed to have occurred in *p*-xylene. Dissociation barrier assumed to equal dissociation cost. Computed free energies converted to 1 M standard state.

predicted by B3LYP-D2 (20.4 kcal/mol at 233 K) is thus considered to be a reasonably reliable estimate. Interestingly, despite the variation in absolute values, all functional combinations consistently predict that the cost of **A1** dissociation is 3 to 4 kcal/mol higher at 233K than at 298K (Table S3), whereas the hydrogenation barriers for all functionals instead are 1 to 2 kcal/mol lower at 233K (Table S2). This implies that the isomerization and hydrogenation barriers at 233K are >5 kcal/mol closer to each other than they are at 298 K for all functionals evaluated. This supports the hypothesis that the selectivity at lower temperatures is influenced by the barrier for isomerization.

Additional benchmark studies of the employed computational protocol (B3LYP-D2, with IEFPCM and basis set settings as in the computational details) on different experimental values are shown in Table 3 (B3LYP-D3 values are also given for comparison). In addition to two experimental values known for the **C1** system (dihydride equilibrium and selectivity at 298 K with **A1**),<sup>10</sup> we studied proton transfer, oxidative addition, and ligand dissociation from three different iridium-pincer complexes.<sup>30,31,32</sup> B3LYP-D2 absolute errors are in the range of 0.3 to 2.5 kcal/mol for all six experimental values, indicating good performance of this protocol. B3LYP-D3 performs less well in several cases and underestimates the ligand dissociation cost significantly (-6.2 kcal/mol).

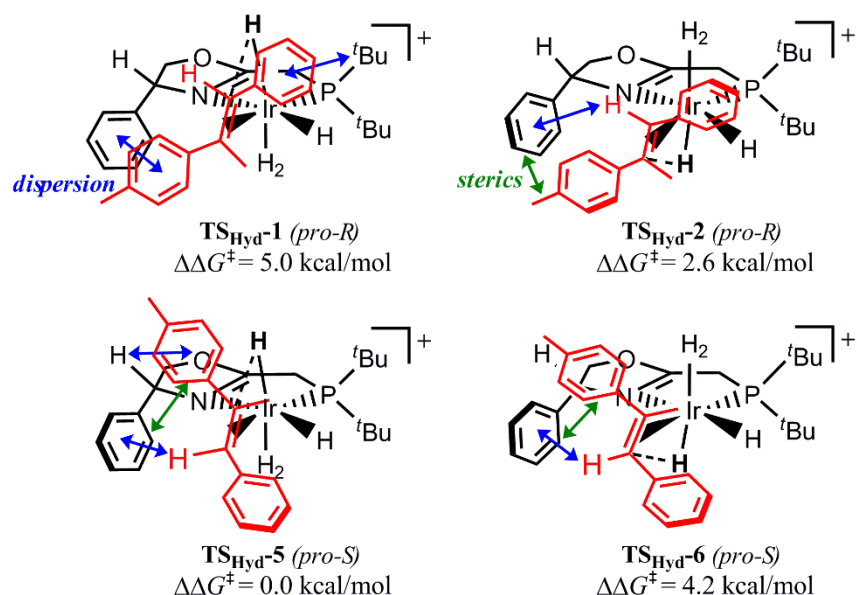


**Figure 8.** Schematic representation of the selectivity-determining interactions at the four lowest-lying hydride transfer transition states for **C1**-mediated hydrogenation of **A1** (blue and green arrows indicate, respectively, dispersion and steric interactions). The hydride transfer path is indicated with a black dashed line. The concomitant oxidative cleavage of  $\text{H}_2$  is omitted for clarity (see also Scheme 1).  $\Delta\Delta G^\ddagger$  values are given relative to the lowest lying TS ( $\text{TS}_{\text{Hyd-5}}$ ).

### Selectivity-determining interactions

The four lowest-lying hydride transfer transition states (formed from **H<sub>2</sub>-DiH-1**, **H<sub>2</sub>-DiH-2**, **H<sub>2</sub>-DiH-5** and **H<sub>2</sub>-DiH-6**) are illustrated schematically in Figure 8. The preferred pro-(*S*) transition state,  $\text{TS}_{\text{Hyd-5}}$ , shows optimal C-H/ $\pi$  dispersion interactions between the substrate hydrogen and the oxazoline phenyl substituent, and between the oxazoline hydrogen, and the tolyl substituent of **A1**. If  $\text{H}_2$  instead is bound above the basal plane and the hydride is transferred from below ( $\text{TS}_{\text{Hyd-6}}$ ), the substrate is displaced such that dispersion interactions with the oxazoline hydrogen vanish, which is reflected in a barrier increase of 4.2 kcal/mol (Fig. 8). For the pro-(*R*) transition states, the preferred geometry ( $\text{TS}_{\text{Hyd-2}}$ ,  $\Delta\Delta G^\ddagger = 2.6$  kcal/mol) shows dispersion interactions between the substrate hydrogen and the oxazoline phenyl substituent, with the substrate displaced such that there is minimal sterics between the oxazoline phenyl and the **A1** tolyl substituent. This orientation is possible, as hydride transfer occurs from below the basal plane. If hydride transfer occurs from above ( $\text{TS}_{\text{Hyd-1}}$ ), the tolyl and the oxazoline phenyl are positioned closer. Although they orient such that favorable stacking interactions can occur, the overall barrier is increased ( $\Delta\Delta G^\ddagger = 5.0$  kcal/mol). The combined results shows that C-H/ $\pi$  dispersion interactions strongly influence the stereochemical outcome.

### In silico design of an improved catalyst

The insights obtained into the mechanistic details and selectivity-determining factors of Ir-PHOX should ideally facilitate the rational design of an improved catalyst. On basis of the transition states optimized in this study, we predict that replacement of the <sup>t</sup>Bu groups of catalyst **C1** with Ph groups (giving catalyst **C2**, Fig. 1) gives improved enantioselectivities for hydrogenation of **A1**. At the lowest-lying hydride-transfer

transition state, this replacement allows for an additional C-H/ $\pi$  dispersion interactions between a hydrogen on the tolyl substituent and a Ph group on phosphorous ( $\text{TS}_{\text{Hyd-5Ph}}$ , Fig. 9 right). At the lowest-lying (*R*)-alkane forming transition state, an analogue interaction is not possible due to a larger distance between **A1** and the Ph substituent. The catalyst modification results in an increased energy gap between the pro-(*R*) and pro-(*S*) pathways with a computed  $\Delta\Delta G^\ddagger_{R-S}$  value of 5.3 kcal/mol (298 K, Figure S5, SI), translating into an *ee* of ~100% (*S*). Interestingly, the synthesis of **C2** has been reported,<sup>2</sup> but to our knowledge, the enantioselectivity of **C2** with a trisubstituted aryl methyl *N*-aryl alkene such as **A1** has not been evaluated experimentally. The experimentally determined *ee* of **C2**-mediated hydrogenation of the tetrasubstituted alkene **A2** is 73% (+),<sup>2</sup> which our calculations are able to reproduce well (computed *ee* of 57% (*R*), 298 K, Figure S6, SI), lending further support to the theoretical predictions provided here.

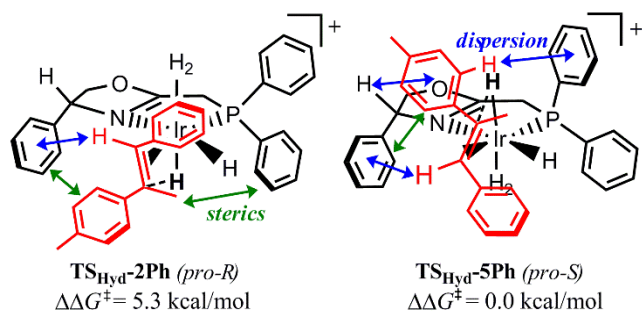


**Figure 9.** Selectivity-determining interactions at the lowest-lying hydride-transfer transition states for **C2**-mediated hydrogenation of **A1**.  $\Delta\Delta G^\ddagger$  values are given relative to  $\text{TS}_{\text{Hyd-5Ph}}$ .



## Conclusions

Hydrogenation of the trisubstituted alkene **A1** with the Ir-PHOX complex **C1** was studied with full quantum chemical models and B3LYP including Grimme empirical dispersion corrections (D2). The results confirm the experimentally observed dihydride species as resting states, but show that these do not give rise to the preferred hydride transfer transition states. Following H<sub>2</sub> binding, it is preferable for both species to isomerize to different intermediates prior to alkene hydrogenation. On basis of the computed  $\Delta\Delta G^\ddagger$  value at 298 K (2.6 kcal/mol), the *ee* is 98 % (*S*) (97 % (*S*) if the reaction kinetics are modeled numerically), in very good agreement with the experimental value reported as 94 % (*S*).<sup>10</sup>

At 233 K, the experimental *ee* is reduced to 72 % (*S*).<sup>10</sup> Our results show that the computed  $\Delta\Delta G^\ddagger$  values are identical at 233 and 298 K (2.6 kcal/mol at both temperatures), i.e. the reduced selectivity at lower temperature should have a different explanation. Interestingly, the computed barrier for dihydride isomerization involving alkene dissociation increases at 233 K, while the hydrogenation barriers decrease, bringing the hydrogenation and isomerization barriers close. We propose that this is a possible origin for the reduced selectivity at lower temperatures. This hypothesis is supported by numerical modeling of the time evolution of the reaction, involving both isomerization and hydrogenation steps.

Analysis of the selectivity-determining interactions at the hydride transfer transition states identifies strong C-H/ $\pi$  type dispersion interactions between substituents on the chiral catalyst carbon (H, Ph) and the substrate substituents (Ph/Tol, H). On basis of the optimized transition states structures, we hypothesize that replacement of the 'Bu substituents with phenyls in the PHOX backbone, yielding catalyst **C2**, could provide improved enantioselectivities for hydrogenation of **A1**. Calculations on **C2**-mediated **A1** hydrogenation support this hypothesis.

Additional benchmark studies of the employed computational protocol against six experimental values (based on iridium-mediated reactions, involving e.g. ligand dissociation, oxidative addition, and proton transfer) show good performance for B3LYP-D2, with absolute errors of 0.3 to 2.5 kcal/mol. This indicates that the computational protocol is very suitable for calculations of this type.

## SUPPORTING INFORMATION

Schematic representation of optimized hydride transfer transition states for **C1**- and **C2**-mediated hydrogenation of **A1** and **A2**, additional hydrogenation mechanisms investigated, analysis of E/Z-isomerization of **A1**, details of the numerical modeling of the reaction kinetics, results for different DFT functionals, further details on benchmark studies, and optimized coordinates in .xyz format in a separate text file (Coordinates\_IrPHOX.xyz) for convenient visualization. This material is available free of charge via the Internet at <http://pubs.acs.org>

## AUTHOR INFORMATION

### Corresponding Author

\* kathrin.hopmann@uit.no.

## ACKNOWLEDGMENTS

This work has been supported by the Research Council of Norway through a FRIPRO grant (No. 231706/F20) to K. H. Hopmann, through a Centre of Excellence Grant (No. 179568/V30), and by the Norwegian Supercomputing Program (NOTUR) through a grant of computer time (No. NN4654K).

## REFERENCES

- Schnider, P.; Koch, G.; Prétôt, R.; Wang, G.; Bohnen, F. M.; Krüger, C.; Pfaltz, A. *Chem. Eur. J.* **1997**, *3*, 887-892.
- Schrems, M. G.; Neumann, E.; Pfaltz, A. *Angew. Chem. Int. Ed.* **2007**, *46*, 8274-8276.
- Baeza, A.; Pfaltz, A. *Chem. Eur. J.* **2010**, *16*, 4003-4009.
- Helmchen, G.; Pfaltz, A. *Acc. Chem. Res.* **2000**, *33*, 336-345.
- Crabtree, R. H.; Felkin, H.; Morris, G. E. *J. Organomet. Chem.* **1977**, *141*, 205.
- Verendel, J.J.; Pàmies, O.; Diéguez, M.; Andersson, P. G. *Chem. Rev.* **2014**, *114*, 2130-2169.
- Brandt, P.; Hedberg, C.; Andersson, P. G. *Chem. Eur. J.* **2003**, *9*, 339-347.
- Hopmann, K.H.; Bayer, A., *Organometallics* **2011**, *30*, 2483-2497.
- Mazet, C.; Smidt, S.P.; Meuwly, M.; Pfaltz, A. *J. Am. Chem. Soc.* **2004**, *126*, 14176-14181.
- Gruber, S., Pfaltz, A. *Angew. Chem. Int. Ed.* **2014**, *53*, 1896-1900.
- Sparta, M.; Riplinger, C.; Neese, F. *J. Chem. Theory Comp.* **2014**, *10*, 1099-1108.
- Church, T. L.; Rasmussen, T.; Andersson, P. G. *Organo-metallics* **2010**, *29*, 6769-6781.
- Grimme, S. *J. Comput. Chem.* **2006**, *27*, 1787-1799.
- Mazuela, J.; Norrby, P.-O.; Andersson, P. G.; Pàmies, O.; Diéguez, M. *J. Am. Chem. Soc.* **2011**, *133*, 13634-13645.
- (a) Becke, A. D. *Phys. Rev. A* **1988**, *38*, 3098-3100, (b) Lee, C.; Yang, W.; Parr, R.G., *Phys. Rev. B* **1988**, *37*, 785-789.
- Gaussian 09 (Revision B.01), Frisch, M.J.; Trucks, G.W.; Schlegel, H.B.; Scuseria, G.E.; Robb, M.A.; Cheeseman, J.R.; Montgomery, Jr., J.A.; Vreven, T.; Kudin, K.N.; Burant, J.C.; Millam, J.M.; Iyengar, S.S.; Tomasi, J.; Barone, V.; Mennucci, B.; Cossi, M.; Scalmani, G.; Rega, N.; Petersson, G.A.; Nakatsuji, H.; Hada, M.; Ehara, M.; Toyota, K.; Fukuda, R.; Hasegawa, J.; Ishida, M.; Nakajima, T.; Honda, Y.; Kitao, O.; Nakai, H.; Klene, M.; Li, X.; Knox, J.E.; Hratchian, H.P.; Cross, J.B.; Bakken, V.; Adamo, C.; Jaramillo, J.; Gomperts, R.; Stratmann, R.E.; Yazyev, O.; Austin, A.J.; Cammi, R.; Pomelli, C.; Ochterski, J.W.; Ayala, P.Y.; Morokuma, K.; Voth, G.A.; Salvador, P.; Dannenberg, J.J.; Zakrzewski, V.G.; Dapprich, S.; Daniels, A.D.; Strain, M.C.; Farkas, O.; Malick, D.K.; Rabuck, A.D.; Raghavachari, K.; Foresman, J.B.; Ortiz, J.V.; Cui, Q.; Baboul, A.G.; Clifford, S.; Cioslowski, J.; Stefanov, B.B.; Liu, G.; Liashenko, A.; Piskorz, P.; Komaromi, I.; Martin, R.L.; Fox, D.J.; Keith, T.; Al-Laham, M.A.; Peng, C.Y.; Nanayakkara, A.; Challacombe, M.; Gill, P.M.W.; Johnson, B.; Chen, W.; Wong, M.W.; Gonzalez, C.; and Pople, J.A., Gaussian, Inc., Wallingford CT.
- (a) Tomasi, J.; Mennucci, B.; Cammi, R. *Chem. Rev.* **2005**, *105*, 2999-3093, (b) Tomasi, J.; Mennucci, B.; Cancès, E. *J. Mol. Struct. (Theochem)* **1999**, *464*, 211-216, (c) Cancès, E.; Mennucci, B.; Tomasi, J. *J. Chem. Phys.* **1997**, *107*, 3032-3041.
- (a) Dunning, T.H. Jr.; Hay, P.J. in *Modern Theoretical Chemistry*, Ed. H.F. Schaefer III, Vol. 3 (Plenum, New York, **1976**) 1-28, (b) Hay, P.J.; Wadt, W.R. *J. Chem. Phys.* **1985**, *82*, 270-283, (c) Hay, P.J.; Wadt, W.R. *J. Chem. Phys.* **1985**, *82*, 284-298, (d) Hay, P.J.; Wadt, W.R. *J. Chem. Phys.* **1985**, *82*, 299-310.
- (a) Roy, L.E.; Hay, P. J.; Martin, R. L. *J. Chem. Theory Comput.* **2008**, *4*, 1029-1031, (b) Ehlers, A. W.; Böhme, M.; Dapprich, S.; Gobbi, A.; Höllwarth, A.; Jonas, V.; Köhler, K. F.; Stegmann, R.; Veldkamp, A.; Frenking, G. *Chem. Phys. Lett.* **1993**, *208*, 111-114.
- Conversion to a 1 M solution standard states can be performed by adding a correction term of 1.89 kcal/mol (298 K, 1.37 kcal/mol at 233 K) to all species. However, given that the hydrogenation reaction was modelled relative to H<sub>2</sub>(g) + DiH-1(aq), it can be discussed whether H<sub>2</sub> should be kept in a 1 atm standard state (which appears more appropriate for a

gas) or not. All energies are therefore reported as computed (1 atm standard state). This should be taken into account when comparing to experimental values.

<sup>21</sup> Cramer, C. J. *Essentials of Computational Chemistry: Theories and Models*, **2002**, p. 183.

<sup>22</sup> Zhao, Y.; Truhlar, D.G., *Theor. Chem. Acc.* **2008**, *120*, 215-241.

<sup>23</sup> Grimme, S.; Antony, J.; Ehrlich, S.; Krieg, H. *J. Chem. Phys.* **2010**, *132*, 154104.

<sup>24</sup> Linear transit calculations with increasing Ir-alkene distance show a continuous increase in the relative energies, i.e. no explicit transition state for alkene dissociation was located. It is possible that such a transition state nonetheless exists, however, it can be assumed that it will closely resemble the dissociated product state and that the activation energy will closely resemble the dissociation energy (see also ref. 25 for a similar discussion in the context of PPh<sub>3</sub> dissociation energies).

<sup>25</sup> Minenkov, Y.; Occhipinti, G.; Jensen, V. R. *J. Phys. Chem. A* **2009**, *113*, 11833-11844.

<sup>26</sup> Fan, Y.; Cui, X.; Burgess, K.; Hall, M. B. *J. Am. Chem. Soc.* **2004**, *126*, 16688-16689.

<sup>27</sup> Perutz, R. N.; Sabo-Etienne, S. *Angew Chem. Int Ed.* **2007**, *46*, 2578-2595.

<sup>28</sup> Sieffert, N.; Bühl, M. *Inorg. Chem.* **2009**, *48*, 4622-4624.

<sup>29</sup> Sparta, M.; Jensen, V. R.; Børve, K. *J. Mol. Phys.*, **2013**, *111*, 1599-1610.

<sup>30</sup> Bernskoetter, W. H.; Hanson, S. K.; Buzak, S. K.; Davis, Z.; White, P. S.; Swartz, R.; Goldberg, K. I.; Brookhart, M. *J. Am. Chem. Soc.* **2009**, *131*, 8603-8613.

<sup>31</sup> Kundu, S. K., *Reactions of (PCP)Ir complexes with small molecules*, Doctoral Dissertation, Rutgers University, Graduate School New Brunswick, **2010**, <http://hdl.rutgers.edu/1782.2/rucore10001600001.ETD.000052125>

<sup>32</sup> Zhao, J.; Goldstein, A. S.; Hartwig, J. F. *Science* **2005**, *307*, 1080-1082.